

First deep search of tidal tails in the Milky Way globular cluster NGC 6362

Andrés E. Piatti^{1,2*}

¹ Instituto Interdisciplinario de Ciencias Básicas (ICB), CONICET-UNCUYO, Padre J. Contreras 1300, M5502JMA, Mendoza, Argentina;

² Consejo Nacional de Investigaciones Científicas y Técnicas (CONICET), Godoy Cruz 2290, C1425FQB, Buenos Aires, Argentina

Received / Accepted

ABSTRACT

I present results of the analysis of a set of images obtained in the field of the Milky Way globular cluster NGC 6362 using the Dark Energy Camera, which is mounted in the 4.0m Victor Blanco telescope of the Cerro-Tololo Interamerican observatory. The cluster was selected as a science case for deep high-quality photometry because of the controversial observational findings and theoretical predictions on the existence of cluster tidal tails. The collected data allowed us to build an unprecedented deep cluster field color-magnitude diagram, from which I filtered stars to produce a stellar density map, to trace the stellar density variation as a function of the position angle for different concentric annuli centered on the cluster, and to construct a cluster stellar density radial profile. I also built a stellar density map from a synthetic color-magnitude diagram generated from a model of the stellar population distribution in the Milky Way. All the analysis approached converge toward a relatively smooth stellar density between 1 and ~ 3.8 cluster Jacobi radii, with a slightly difference smaller than 2 times the background stellar density fluctuation between the mean stellar density of the south-eastern and that of north-western hemispheres, the latter being higher. Moreover, the spatial distribution of the recently claimed tidal tail stars agrees well not only with the observed composite star field distribution, but also with the region least affected by interstellar absorption. Nevertheless, I detected a low stellar density excess around the cluster Jacobi radius, from which I conclude that NGC 6362 present a thin extra tidal halo.

Key words. globular clusters:general – globular clusters:individual:NGC 6362 – methods: observational – techniques:photometric

1. Introduction

The recent stringent compilation of Milky Way globular clusters with robust detections of extra-tidal structures includes only one bulge/disk globular cluster with tidal tails (NGC 6362, Zhang et al. 2022); while Carlberg & Grillmair (2021) do not include any bulge globular cluster in their search for dark matter in the globular clusters' outskirts. This brief overview illustrates that bulge globular clusters have not generally been targeted for studies of their outermost stellar structures, which are fundamental for our understanding of whether they formed in dark matter minihaloes (Starkman et al. 2020; Baumgardt & Vasiliev 2021; Wan et al. 2021); their association to destroyed dwarf progenitors (Carballo-Bello et al. 2014; Mackey et al. 2019); their dynamical history as a consequence of the interaction with the Milky Way (Hozumi & Burkert 2015; de Boer et al. 2019; Piatti & Carballo-Bello 2020), etc. Therefore, there are strong motivations for detecting/characterizing tidal tails in bulge globular clusters, making it a compelling field of research.

Zhang et al. (2022) classified NGC 6362 as a globular cluster with tidal tails based on the work by Kundu et al. (2019), who found 259 of them spread over an area of ~ 4.1 deg² centered on the cluster. These stars should be placed beyond the cluster's Jacobi radius (r_J), which defines the surface from which cluster stars are not longer bounded to the cluster and are lost in the form of tidal tails. The value of r_J depends on the Milky Way potential at the position of the globular and its orbit around the

Milky Way. For NGC 6362, Piatti et al. (2019) derived $r_J = 0.26$ deg. Kundu et al. (2019) also showed that the cluster is moving in a chaotic orbit. However, Mestre et al. (2020) compared the behavior of simulated streams embedded in chaotic and non-chaotic regions of the phase-space and found that typical gravitational potentials of host galaxies can sustain chaotic orbits, which in turn do reduce the time interval during which streams can be detected. This explains why tidal tails in some globular clusters are washed out afterwards they are generated to the point at which it is impossible to detect them. Indeed, NGC 5139, with an apogalactocentric distance of 7.0 kpc, is the innermost globular cluster with observed tidal tails; NGC 6362 is at 5.5 kpc from the Galactic center (Baumgardt & Vasiliev 2021).

Given that the structures I am interested in –the tidal tails of NGC 6362– are mainly composed of low-mass Main Sequence stars, it is necessary to map the faint end of the cluster color-magnitude diagram (CMD), allowing us to determine the outer structure of the cluster with excellent statistics and to truly map the outskirts to look for tidal tails. It is widely accepted that Milky Way globular clusters have lost most of their masses through three main processes, namely: stellar evolution, two-body relaxation and tidal heating caused by the Milky Way's gravitational field (Piatti et al. 2019, and reference therein). Studies on the external regions of Milky Way globular clusters use such faint Main Sequence stars to detect tidal tails, because they are more numerous (Carballo-Bello et al. 2012). I note that the *Gaia* data used by Kundu et al. (2019) to select tidal tail stars barely reach the cluster's Main Sequence turnoff ($G_0 \sim 19$ mag).

* e-mail: andres.piatti@fcen.uncu.edu.ar

In Section 2 I describe the deep wide-field observations carried out to investigate the existence of tidal tails in the outskirts of NGC 6362. The analysis of the obtained CMD and stellar density maps is described in Section 3, while Section 4 deals with the discussion of the present outcomes to the light of our knowledge of the distribution of stars and gas in the Milky way along the cluster’s line-of-sight. In Section 5 I summarize the main conclusions of this work.

2. Observational data

I employed the Dark Energy Camera (DECam, Flaugher et al. 2015), an array of 62 identical chips with a scale of $0.263 \text{ arcsec pixel}^{-1}$ that provides a 3 deg^2 field of view, attached to the prime focus of the 4-m Blanco telescope at the Cerro Tololo Inter-American Observatory (CTIO). The collected data are part of the observing program 2023A-627924 (PI: A. Piatti) and consist of $4 \times 400s$ g and $1 \times 100s + 7 \times 400s$ i exposures, respectively. The images’ quality resulted to be better than 0.9 arcsec . The DECam community pipeline processed the images by applying the highest performance instrumental calibrations, eliminating one CCD of problematic usefulness. The CCD images were trimmed of bad edge pixels, and reference bias and dome flat files were created for each night in order to remove the instrumental signature from the science data. The images were then resampled to a standard orientation and pixel scale at a standard tangent point. Finally, the DECam community pipeline applied photometric calibrations.

I split the entire DECam field of view in nine equal squared areas of $\sim 0.67 \text{ deg}$ a side, and for each of these sub-fields I performed point spread function (PSF) photometry using the DAOPHOT/ALLSTAR suite of programs (Stetson et al. 1990). For each sub-field, I obtained a quadratically varying PSF by fitting $\sim 2200 \text{ stars deg}^2$, once I eliminated the neighbors using a preliminary PSF derived from the brightest, least contaminated 900 stars deg^2 . Both groups of PSF stars were interactively selected. We then used the ALLSTAR program to apply the resulting PSF to the identified stellar objects and to create a subtracted image, which was used to find and measure magnitudes of additional fainter stars. This procedure was repeated three times for each sub-field. In order to properly match a g sub-field with the corresponding i one, I used the IRAF/IMMATCH@WCSMAP task, and then stand-alone DAOMATCH/DAOMASTER routines¹ to gather pixel coordinates, g and i magnitudes with their respective errors, sharpness and χ values for all the measured sources. Finally, I assigned R.A. and Dec. coordinates to each stars using the wcstool package² and kept sources with $|\text{sharpness}| < 0.5$ in order to remove bad pixels, unresolved double stars, cosmic rays, and background galaxies from the photometric catalog.

3. Data analysis

The region onto which NGC 6362 is projected is affected by interstellar extinction that varies with the position in the sky. In order to reproduce the interstellar extinction map towards the cluster, I retrieved the $E(B - V)$ values as a function of R.A. and Dec. from Schlafly & Finkbeiner (2011), provided by the NASA/IPAC Infrared Science Archive³ for the entire analyzed area. Figure 1 illustrates the resulting extinction map, which reveals that along the cluster’s line-of-sight the interstellar absorp-

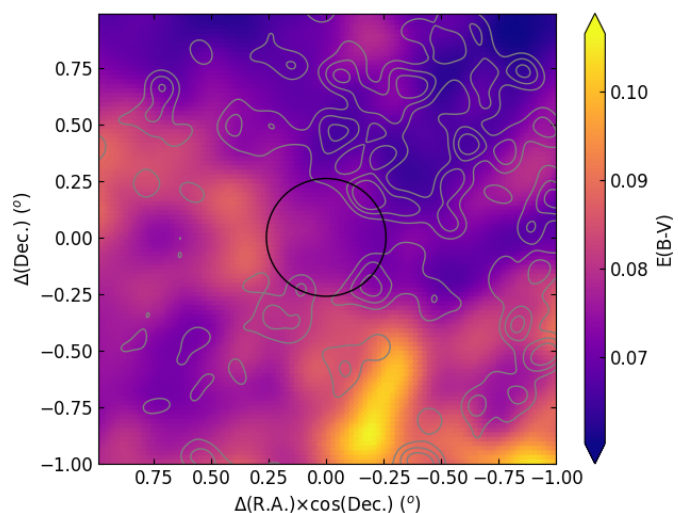


Fig. 1. Interstellar extinction ($E(B - V)$) map across the observed NGC 6362 field. The black circle represents the cluster’s Jacobi radius (0.26 deg), while the gray contours correspond to isodensity levels of the tidal tail stars selected by Kundu et al. (2019).

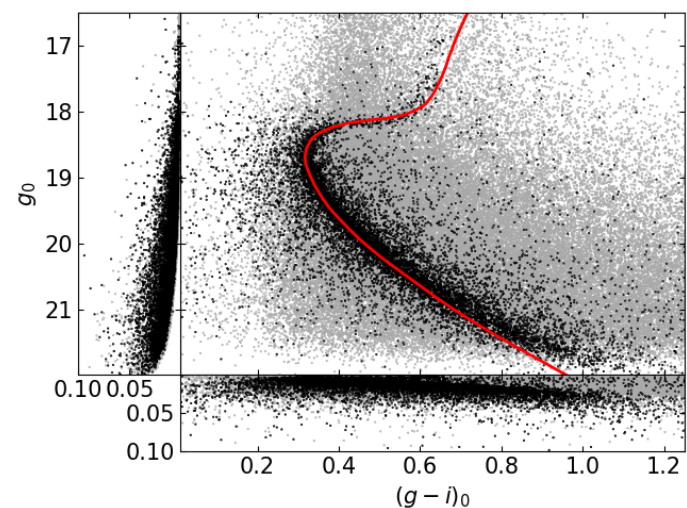


Fig. 2. CMD for all the measured stars in the field for NGC 6362, with their respective photometric errors. Black and gray dots represent stars located inside/outside a circle of radius equals to 2 times the cluster’s half-mass radius (0.11 deg), respectively. The red line is an isochrone for the cluster’s age (12 Gyr) and metallicity ($[\text{Fe}/\text{H}] = -1.07 \text{ dex}$) (Gontcharov et al. 2023).

tion is relatively low, with a maximum difference between the most and least reddened regions of $\Delta E(B - V) \lesssim 0.05 \text{ mag}$. Based on Figure 1, I assigned individual $E(B - V)$ values to the measured stars according to their positions in the sky. In order to correct the observed magnitudes and colors by interstellar extinction, I used the individual $E(B - V)$ values and the A_1/A_V coefficients given by Wang & Chen (2019). Figure 2 shows the wealth of information that I produced from the observed images, where a nearly 3 mag long well-defined cluster’s Main Sequence is clearly visible, alongside with the cluster’s Main Sequence Turnoff, sub-giant and the fainter segment of the giant branches. In order to highlights the cluster’s CMD features I used all the measured stars located within a circle of radius equal to two times the cluster’s half-mass radius ($r_h = 0.11 \text{ deg}$, Baumgardt & Vasiliev 2021). The positions of stars located inside $2 \times r_h$ are satisfactorily reproduced by an isochrone (Bressan et al. 2012) for

¹ programs kindly provided by P.B. Stetson

² <http://tdc-www.harvard.edu/wcstools/>

³ <https://irsa.ipac.caltech.edu/>

the cluster's age (12 Gyr) and metallicity ($[Fe/H] = -1.07$ dex) (Gontcharov et al. 2023). Figure 2 also shows that the photometric uncertainties of magnitude and color for the faintest observed cluster's stars are smaller than ~ 0.05 mag. NGC 6362 appears projected onto a crowded star field (gray dots in Figure 2).

The strategy chosen to uncover the spatial distribution of stars that formed within NGC 6362 and are now observed beyond its Jacobi radius consists in to statistically identify cluster's Main Sequence stars located outside that radius, following the recipe outlined by Zhang et al. (2022). For that purpose, I firstly defined a region along the cluster's Main Sequence, from $g_0 = 18$ mag down to $g_0 = 21.5$ mag, and secondly, I built a stellar density map for all the stars that fall within that CMD region. Unfortunately, this approach is not able to discern on the cluster membership of these stars. For such an assessment, I need additional information such as proper motions, radial velocities, metallicities, among others. As far as I am aware, because of the relative faintness of the involved stars, this piece of information is still unavailable. Nevertheless, field stars within the cluster's Main Sequence region are expected to be distributed throughout the entire field, so that cluster stars arise as particular shaped stellar overdensities forming an extended envelope, extra-tidal debris or tidal tails (Piatti & Carballo-Bello 2020).

The cluster's Main Sequence region was devised from the following two steps. I first traced the cluster's Main Sequence ridge line, and then, I fixed the color width of the devised region as a function of the magnitude. Both steps were carried out using the stars located within $2 \times r_h$ from the cluster center, i.e., those black points in Figure 2. The cluster's Main Sequence ridge line was determined by computing the median of the color distribution for magnitude intervals of $\Delta g_0 = 0.1$ mag, while their widths correspond to the derived color standard deviations. Figure 3 depicts a Hess diagram for the employed stars and the various generated curved, namely: the cluster's Main Sequence ridge line (red), the lower and upper limits of the cluster's Main Sequence colors (orange), and the cluster's Main Sequence limits (magenta) corresponding to the mode of the color error distribution (see, also, the trend of errors in Figure 2). As can be seen, the photometric errors are notably smaller than the adopted intrinsic width of the cluster's Main Sequence.

I made use of the `scikit-learn` software machine learning library (Pedregosa et al. 2011) and its Gaussian kernel density estimator (KDE) to build the stellar density map for the observed field around NGC 6362, using all the stars distributed within the cluster's Main Sequence region. I employed a grid of 500×500 boxes onto the DECam field and used a range of values for the bandwidth from 0.01° up to 0.1° in steps of 0.01° in order to apply the KDE to each generated box. I adopted a bandwidth of 0.05° as the optimal value, as guided by `scikit-learn`. Figure 4 shows the resulting density map, where I used a maximum level of 2 stars arcmin^{-2} in order to highlight lower density levels. The observed spatial pattern of stars located in the cluster's Main Sequence region shows a nearly rounded distribution inside the Jacobi radius and no obvious trail of tidal tails outside it, but a nearly smooth stellar distribution over the entire observed field, as expected for a composite star field population. With the aim of quantifying such a trend, I used three different concentric annuli around the cluster center and measured the stellar densities in angular sectors of 10 deg wide. The upper panel of Figure 5 illustrates the behavior of the stellar density as a function of the position angle, measured from North to East. As can be seen, the three stellar density profiles around the cluster are similar, with fluctuations that mostly vary around a mean value of 0.48 stars arcmin^{-2} in an amount of $\sigma = 0.11$ stars arcmin^{-2} .

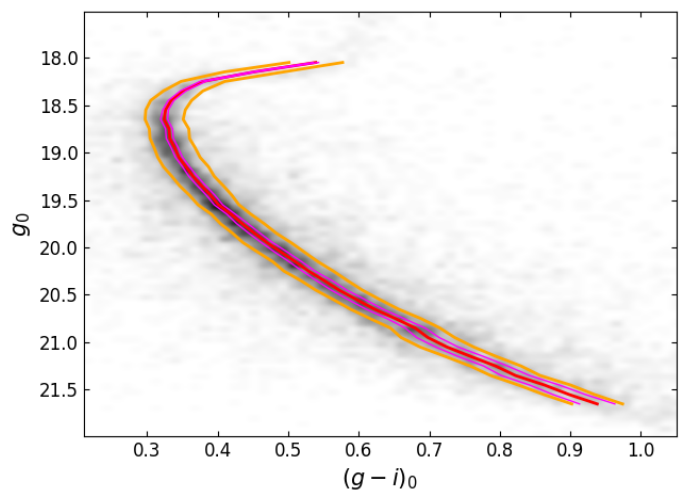


Fig. 3. Hess diagram for the stars located within $2 \times r_h$ from the cluster center. The traced cluster's Main Sequence ridge line (red), its defined lower and upper color limits (orange), and those corresponding to the mode of the color error distribution (magenta) are superimposed, respectively.

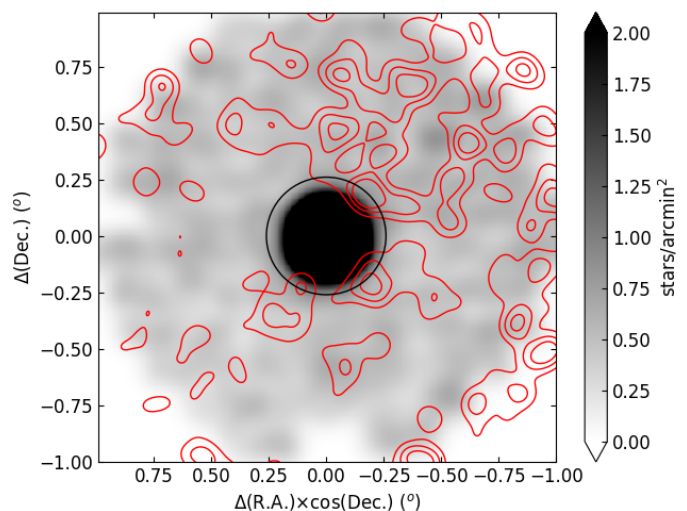


Fig. 4. Stellar density map of stars distributed within the cluster's Main Sequence region. The black circle represents the cluster's Jacobi radius, while the red contours correspond the stellar density levels of stars selected by Kundu et al. (2019) (see Figure 6).

I then computed the deviation from the mean value in the field in units of the standard deviation, that is, $\eta = (\text{signal} - \text{mean value}) / \text{standard deviation}$. From the bottom panel of Figure 5, I infer that there are some regions, located particularly in the outer north-western hemisphere, with $\eta \gtrsim 2$, which implies a significance level larger than 95%.

4. Analysis and discussion

Kundu et al. (2019) selected cluster stars ($g_0 \lesssim 18.0$ mag) located beyond its Jacobi radius based on astrometry filtering criteria. They appear in the CMD distributed along the cluster sub-giant and red giant branches, and horizontal branch as well. Particularly, Kundu et al. (2019) restricted cluster stars to have proper motions within 3σ from the mean cluster proper motion. This criterion, which is helpful for identifying cluster stars within the cluster body, could fail when applying to stars formed in the clus-

ter that have later abandoned it. This is because of tidal tail stars have speed up their pace in order to escape the cluster. There are, additionally, other reasons that can contribute to make the proper motion of tidal tail stars different from the mean cluster proper motion, among them, projection effects of the tidal tails, the Milky Way tidal interaction, the intrinsic kinematic agitation of a stellar stream (Wan et al. 2023). Likewise, it is possible to find field stars projected along the cluster line of sight that share proper motions similar to cluster stars (Piatti et al. 2023).

I used the *Gaia* DR2 data (Gaia Collaboration et al. 2016, 2018) from Kundu et al. (2019) for their selected 259 extra-tidal stars to build a stellar density map following the same precepts described above to construct Figure 4. Figure 6 shows the resulting stellar density map, to which I also traced different contour levels. The stars seem to be preferentially distributed across the north-western hemisphere, where I also unveiled a slightly excess with respect to the south-eastern hemisphere ($\Delta\eta \sim 2$) for stars located along the cluster’s Main Sequence region ($g_0 > 18.0$ mag). This means that, independently of the chosen magnitude range along the cluster CMD, stars distributed across the observed DECam field following a similar spatial pattern. I also note that Figure 2 reveals a large population of field stars superimposed onto the cluster CMD features (background gray dots). As for comparison purposes, I overplotted the contour levels of Kundu et al. (2019)’s stars onto the stellar density map of the cluster’s Main Sequence stars (see Figure 4), and onto the reddening map (see Figure 1). Their spatial distribution could suggest that they are confined within the lower reddening regions. Nevertheless, the variation of the reddening across the field is not so high ($\Delta E(B - V) \lesssim 0.05$ mag) as to expect a variation in the stellar density of these relatively bright stars due to interstellar absorption.

How to discern whether the spatial distribution of the stars selected by Kundu et al. (2019) really represent extra-tidal features of NGC 6362? If they were confirmed, then the slightly stellar excess found from stars distributed within the cluster’s Main Sequence region could also be an evidence of the presence of such extra-tidal structures. Furthermore, they would be very low stellar density tidal tails that do not surpass $\eta = 3$. According to Piatti & Carballo-Bello (2020), Milky Way globular clusters can exhibit tidal tails, extended envelopes or do not show any extra-tidal structures. When I examine the shapes of extra-tidal structures of nearly 50 studied globular clusters (Zhang et al. 2022, and references therein), I conclude that extended envelope stellar distributions are functions of the distance to the cluster center, no angular direction arises as preferential. In turn, tidal tails are well collimated stellar structures that emerge from the cluster body in two directions, namely, the leading and the trailing tails, respectively. Unfortunately, neither an extended envelope nor tidal tails can be recognized from the spatial distribution of stars selected by Kundu et al. (2019) and in this work (see Figure 4).

The presence of tidal tails in some globular clusters and the absence of them in others is still a topic of debate. Piatti & Carballo-Bello (2020) explored different kinematical and structural parameter spaces, and found that globular clusters behave similarly, irrespective of the presence of extended envelopes or tidal tails, or the absence thereof. Zhang et al. (2022) showed that globular clusters with tidal tails or extended envelopes have apogalactocentric distances $\gtrsim 5$ kpc, a behavior previously noticed by Piatti (2021), who suggested that the lack of detection of tidal tails in bulge globular clusters could be due to the reduced diffusion time of tidal tails by the kinematically chaotic nature of the orbits of these globular clusters (Kundu et al. 2019),

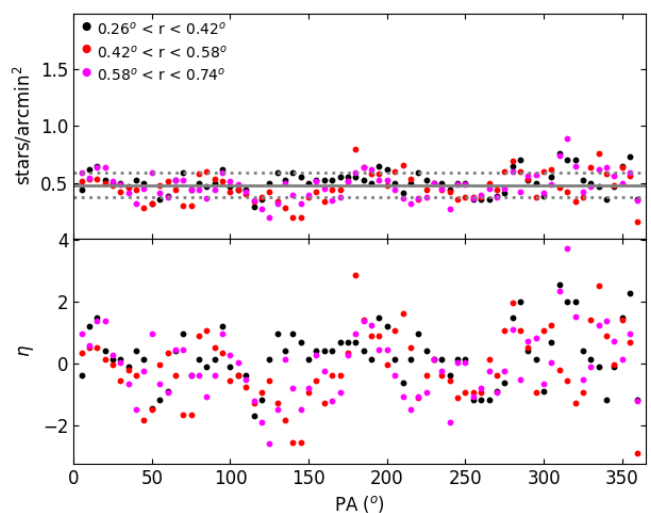


Fig. 5. Stellar density as a function of the position angle for three different concentric annuli centered on NGC 6362, as indicated in the top panel. The solid and dotted lines represent the mean and standard deviation of all the plotted points. The significance (η) of the stellar density over the mean background value is depicted in the bottom panel.

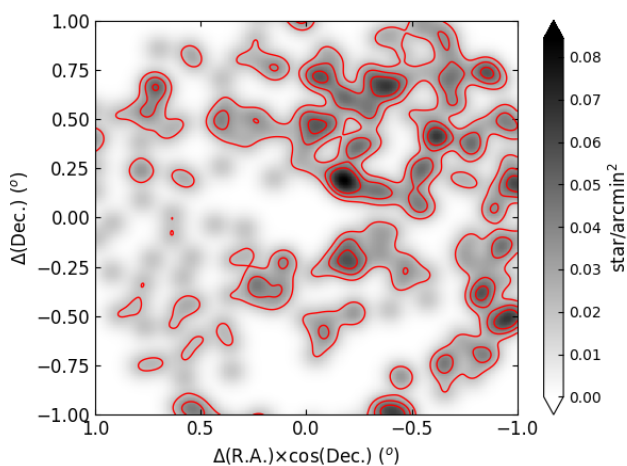


Fig. 6. Stellar density map for the tidal tail stars selected by Kundu et al. (2019), with contour levels corresponding to 0.02, 0.035, and 0.05 stars arcmin^{-2} .

thus shortening the time interval during which the tidal tails can be detected. Recently, Weatherford et al. (2023) re-examined the behavior of potential escapers in globular clusters dynamically evolving along chaotic orbits and found diffusion times smaller than 100 Myr. NGC 6362 is a dynamically evolving globular cluster with a significant internal rotation (Dalessandro et al. 2021).

I investigated the possibility that the spatial distribution of Kundu et al. (2019)’s selected stars (see Figure 6) can be due to the expected stellar density of Milky Way field stars along the cluster’s line of sight. For that purpose, I made use of TRILEGAL⁴ (Girardi et al. 2005), a stellar population synthesis code that allows changes in the star formation rate, age-metallicity relation, initial mass function, geometry of Milky Way components, among others. I used 81 adjacent squared regions of 0.0625 deg^2 each, that cover uniformly the entire observed DE-

⁴ <http://stev.oapd.inaf.it/cgi-bin/trilegal>

Cam field. I generated individual CMDs for each sub-field and then counted the number of stars located within the cluster's Main Sequence region, similarly as we did to build Figure 4.

I chose the DECam photometric system, a limiting magnitude of $g, i = 23$ mag, and a distance modulus resolution of the Milky Way components of 0.1 mag. I set the initial mass function according to Kroupa (2002), a binary fraction of 0.3 with a mass ratio larger than 0.7. The interstellar extinction was modeled by an exponential disk with a scale height $h_z = 100$ pc and a scale length $h_R = 3200$ pc and a visual absorption variation $\partial A_V/\partial R = 0.00015$ mag/pc (Li et al. 2018), and the Sun position at $R_\odot = 8300$ pc, and $z_\odot = 15$ pc (Monteiro et al. 2021). The Milky Way halo, thin and thick disks, and bulge were modeled as follows: the halo was represented by an oblate $r^{1/4}$ spheroid with an effective radius $r_h = 2698.93$ pc and an oblateness $q_h = 0.583063$, and $\Omega = 0.0001 M_\odot/\text{pc}^3$. The halo star formation rate and age-metallicity relationship are those given by (Ryan & Norris 1991). The thin disk is described by an exponential disk along z and R , respectively, with a scale height increasing with the age: $h_z = 94.690 \times (1 + \text{age}/5.55079 \times 10^9)^{1.6666}$, and a scale length $h_R = 2913.36$ pc and an outer cutoff at 15000 pc. We used a 2-step star formation rate, the age-metallicity relationship with α -enrichment given by Fuhrmann (1998), and $\Sigma = 55.4082 M_\odot/\text{pc}^2$. The thick disk is also represented by an exponential disk in both z and R directions, with scale height $h_z = 800$ pc, and scale length $h_R = 2394.07$ pc and outer cutoff at 15000 pc; $\Omega = 0.001 M_\odot/\text{pc}^3$. I adopted a constant star formation rate and $Z = 0.008$ with $\sigma[M/H] = 0.1$ dex. Finally, I assumed a triaxial bulge with a scale length of 2500 pc and a truncation scale length of 95 pc, and y/x and z/x axial ratios of 0.68 and 0.31, respectively. The angle between the direction along the bar and that from the Sun to the Milky Way center was set in 15 deg, and $\Omega = 406 M_\odot/\text{pc}^3$. Its star formation rate and age-metallicity relationship were taken from Zoccali et al. (2003).

Figure 7 illustrates the resulting synthetic CMD for the entire studied field, which compares well with that obtained from the observed DECam field (see Figure 2); while Figure 8 depicts the stellar density map built from TRILEGAL stars distributed within the cluster's Main Sequence region. At a first glance, there is a similarity between the synthetic stellar density map and the spatial distribution of the stars selected by Kundu et al. (2019), which poses the possibility that they could belong to the composite star field population rather than being NGC 6362 tidal tail stars.

I finally built the cluster stellar density radial profile using the stars distributed within the Main Sequence region. I counted the number of stars distributed inside boxes of 0.01 deg up to 0.05 deg a side, increasing by steps of 0.01 deg a side, and then built the corresponding radial profiles. This procedure allowed us to extend the radial profile far from the cluster center, where the area of the observed DECam field do not cover entirely those of concentric annulii centered on the cluster. The resulting average radial profile is depicted with open circles in Figure 9. As expected, the background level is clearly visibly across an extended region. I then subtracted to the observed radial profile the mean value of the background stellar density derived above and superimposed to that background corrected radial profile (filled circles) a King (1962)'s profile with core and tidal radius taken from Baumgardt & Hilker (2018). As can be seen, the King (1962)'s profile matches very well the cluster radial profile, which exhibits around the distance of the cluster's Jacobi radius an excess of stars following a power law distribution with an slope of 4.0. The latter is remarkably different from the values obtained for Milky Way globular clusters with

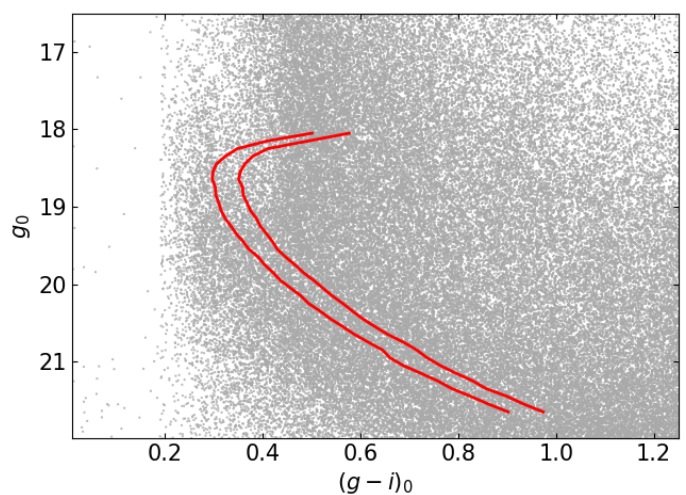


Fig. 7. Synthetic CMD generated using TRILEGAL for the studied Milky Way region (see text for details). The red lines represent the devised cluster's Main Sequence region.

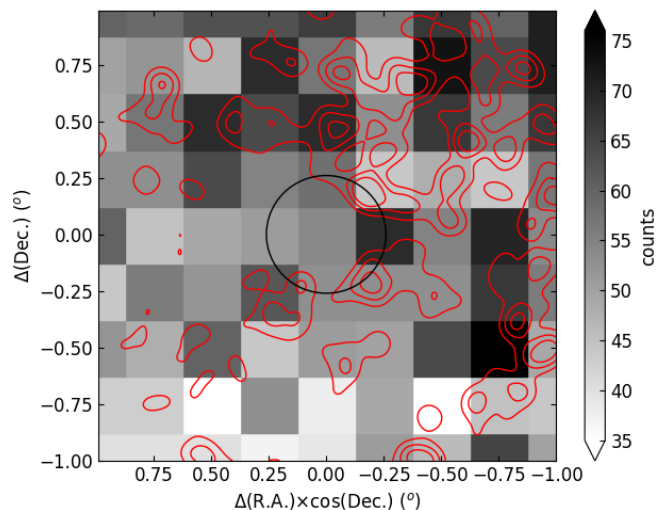


Fig. 8. Stellar density map built from star counts of stars distributed within the cluster's Main Sequence region generated using TRILEGAL (see text for details). The red contour levels represent the spatial distribution of stars selected by Kundu et al. (2019). The black circle represent the cluster's Jacobi radius.

extended envelopes (slope ~ 1 ; e.g., Olszewski et al. 2009; Piatti 2017). Although the deviation of the radial profile from the King (1962)'s profile is visible, I argue that it does not reveal an extended envelope, but a thin not-uniform low stellar density halo. This outcome is in very good agreement with the slightly difference found between the north-western and south-eastern outer hemispheres from the stellar density map.

5. Conclusions

The study of the outermost regions of Milky Way globular clusters is interesting by its own, since it provides clues about a variety of astrophysical topics for which our understanding is far from being complete (see Section 1). According to a recent study, NGC 6362 presents tidal tails out to ~ 2 deg from its center (Kundu et al. 2019), which challenges theoretical predictions for globular clusters in chaotic orbit regimes, and orbiting close to the Milky Way bulge. I recognized here a science case, and

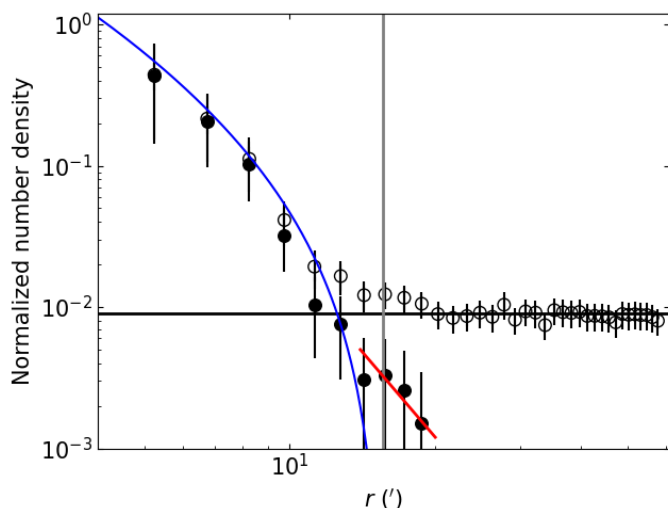


Fig. 9. Observed and background corrected normalized stellar density profiles represented by open and filled circles, respectively. Error bars are also shown. The blue curve represents the King’s model for the core and tidal radius of the cluster (Baumgardt & Hilker 2018); while the red line corresponds to a power law with slope equals to 4.0. Black horizontal and gray vertical lines represent the mean background level and the cluster Jacobi radius, respectively.

embarked in the first deep search for extra tidal stars throughout an extended region around the cluster.

The collected data consist of images obtained with the 4.0m Blanco telescope (CTIO) that reach nearly 3 mag below the cluster’s Main Sequence turnoff across an area of $\sim 3 \text{ deg}^2$, a limiting magnitude not achieved by any ground-based observation, but only by HST data (Dalessandro et al. 2014) for the innermost cluster region. I scrutinized the produced DECam field CMD, from which I selected stars distributed across the entire field and encompassed within the devised cluster’s Main Sequence region. Using those stars we built a stellar density map, an azimuthal stellar distribution for different concentric annuli centered on the cluster, and a cluster stellar density radial profile. From the stellar density map, I detected an overall relatively smooth stellar density distribution from the cluster Jacobi radius out to nearly $3.8 \times r_J$, with a slightly difference smaller than 2 times the background stellar density fluctuation between the mean stellar density of the south-eastern and that of north-western hemispheres, the latter being higher. The same trend is observed in the plane of the stellar density as a function of the position angle, and from the stellar radial profile. I finally constructed a stellar density map from a synthetic CMD generated from a model of the stellar population distribution in the Milky Way, which also confirms the above findings.

On the other hand, I produced a stellar density map of the tidal tail stars selected by Kundu et al. (2019) and superimposed the corresponding contour levels over the present stellar density map and that obtained from the synthetic CMD. The Kundu et al. (2019)’s tidal tail stars are distributed mainly throughout the north-western hemisphere, which suggests that they likely belong to the composite star field population. I also examined their spatial distribution with that of the interstellar absorption toward the cluster, and found that they are projected onto the least reddened regions. Nevertheless, I detected a low stellar density excess around the cluster Jacobi radius, from which I conclude that NGC 6362 present a thin extra tidal halo. This outcome is two-fold in very good agreement with the expected relative high clus-

ter star mass lost by disruption (Piatti et al. 2019) and the short diffuse time of tidal tails applicable to this globular cluster.

Acknowledgements. I thank the referee for the thorough reading of the manuscript and timely suggestions to improve it. This project used data obtained with the Dark Energy Camera (DECam), which was constructed by the Dark Energy Survey (DES) collaboration. Funding for the DES Projects has been provided by the US Department of Energy, the US National Science Foundation, the Ministry of Science and Education of Spain, the Science and Technology Facilities Council of the United Kingdom, the Higher Education Funding Council for England, the National Center for Supercomputing Applications at the University of Illinois at Urbana-Champaign, the Kavli Institute for Cosmological Physics at the University of Chicago, Center for Cosmology and Astro-Particle Physics at the Ohio State University, the Mitchell Institute for Fundamental Physics and Astronomy at Texas A&M University, Financiadora de Estudos e Projetos, Fundação Carlos Chagas Filho de Amparo Pesquisa do Estado do Rio de Janeiro, Conselho Nacional de Desenvolvimento Científico e Tecnológico and the Ministério da Ciência, Tecnologia e Inovação, the Deutsche Forschungsgemeinschaft and the Collaborating Institutions in the Dark Energy Survey. The Collaborating Institutions are Argonne National Laboratory, the University of California at Santa Cruz, the University of Cambridge, Centro de Investigaciones Energéticas, Medioambientales y Tecnológicas–Madrid, the University of Chicago, University College London, the DES-Brazil Consortium, the University of Edinburgh, the Eidgenössische Technische Hochschule (ETH) Zürich, Fermi National Accelerator Laboratory, the University of Illinois at Urbana-Champaign, the Institut de Ciències de l’Espai (IEEC/CSIC), the Institut de Física d’Altes Energies, Lawrence Berkeley National Laboratory, the Ludwig-Maximilians Universität München and the associated Excellence Cluster Universe, the University of Michigan, NSF’s NOIRLab, the University of Nottingham, the Ohio State University, the OzDES Membership Consortium, the University of Pennsylvania, the University of Portsmouth, SLAC National Accelerator Laboratory, Stanford University, the University of Sussex, and Texas A&M University. Based on observations at Cerro Tololo Inter-American Observatory, NSF’s NOIRLab (NOIRLab Prop. ID 2023A-627924; PI: A. Piatti), which is managed by the Association of Universities for Research in Astronomy (AURA) under a cooperative agreement with the National Science Foundation. Data for reproducing the figures and analysis in this work will be available upon request to the author.

References

- Baumgardt, H. & Hilker, M. 2018, *MNRAS*, 478, 1520
 Baumgardt, H. & Vasiliev, E. 2021, *MNRAS*, 505, 5957
 Bressan, A., Marigo, P., Girardi, L., et al. 2012, *MNRAS*, 427, 127
 Carballo-Bello, J. A., Gieles, M., Sollima, A., et al. 2012, *MNRAS*, 419, 14
 Carballo-Bello, J. A., Sollima, A., Martínez-Delgado, D., et al. 2014, *MNRAS*, 445, 2971
 Carlberg, R. G. & Grillmair, C. J. 2021, *ApJ*, 922, 104
 Dalessandro, E., Massari, D., Bellazzini, M., et al. 2014, *ApJ*, 791, L4
 Dalessandro, E., Raso, S., Kamann, S., et al. 2021, *MNRAS*, 506, 813
 de Boer, T. J. L., Gieles, M., Balbinot, E., et al. 2019, *MNRAS*, 485, 4906
 Flaugher, B., Diehl, H. T., Honscheid, K., et al. 2015, *AJ*, 150, 150
 Fuhrmann, K. 1998, *A&A*, 338, 161
 Gaia Collaboration, Brown, A. G. A., Vallenari, A., et al. 2018, *A&A*, 616, A1
 Gaia Collaboration, Prusti, T., de Bruijne, J. H. J., et al. 2016, *A&A*, 595, A1
 Girardi, L., Groenewegen, M. A. T., Hatziminaoglou, E., & da Costa, L. 2005, *A&A*, 436, 895
 Gnedin, O. Y. & Ostriker, J. P. 1997, *ApJ*, 474, 223
 Gontcharov, G. A., Khovritchev, M. Y., Mosenkov, A. V., et al. 2023, *MNRAS*, 518, 3036
 Hozumi, S. & Burkert, A. 2015, *MNRAS*, 446, 3100
 King, I. 1962, *AJ*, 67, 471
 Kroupa, P. 2002, *Science*, 295, 82
 Kundu, R., Fernández-Trincado, J. G., Minniti, D., et al. 2019, *MNRAS*, 489, 4565
 Li, L., Shen, S., Hou, J., et al. 2018, *ApJ*, 858, 75
 Mackey, A. D., Ferguson, A. M. N., Huxor, A. P., et al. 2019, *MNRAS*, 484, 1756
 Mestre, M., Llinares, C., & Carpintero, D. D. 2020, *MNRAS*, 492, 4398
 Monteiro, H., Barros, D. A., Dias, W. S., & Lépine, J. R. D. 2021, *Frontiers in Astronomy and Space Sciences*, 8, 62
 Olszewski, E. W., Saha, A., Knezek, P., et al. 2009, *AJ*, 138, 1570
 Pedregosa, F., Varoquaux, G., Gramfort, A., et al. 2011, *Journal of Machine Learning Research*, 12, 2825
 Piatti, A. E. 2017, *MNRAS*, 466, 4960
 Piatti, A. E. 2021, *MNRAS*, 505, 3033
 Piatti, A. E. & Carballo-Bello, J. A. 2020, *A&A*, 637, L2
 Piatti, A. E., Illesca, D. M. F., Massara, A. A., et al. 2023, *MNRAS*, 518, 6216

- Piatti, A. E., Webb, J. J., & Carlberg, R. G. 2019, *MNRAS*, 489, 4367
- Ryan, S. G. & Norris, J. E. 1991, *AJ*, 101, 1865
- Schlafly, E. F. & Finkbeiner, D. P. 2011, *ApJ*, 737, 103
- Starkman, N., Bovy, J., & Webb, J. J. 2020, *MNRAS*, 493, 4978
- Stetson, P. B., Davis, L. E., & Crabtree, D. R. 1990, in *Astronomical Society of the Pacific Conference Series*, Vol. 8, *CCDs in astronomy*, ed. G. H. Jacoby, 289–304
- Wan, Z., Arnold, A. D., Oliver, W. H., et al. 2023, *MNRAS*, 519, 192
- Wan, Z., Oliver, W. H., Baumgardt, H., et al. 2021, *MNRAS*, 502, 4513
- Wang, S. & Chen, X. 2019, *ApJ*, 877, 116
- Weatherford, N. C., Rasio, F. A., Chatterjee, S., et al. 2023, *arXiv e-prints*, arXiv:2310.01485
- Zhang, S., Mackey, D., & Da Costa, G. S. 2022, *MNRAS*, 513, 3136
- Zoccali, M., Renzini, A., Ortolani, S., et al. 2003, *A&A*, 399, 931